Docket No. SA-509

Exhibit No. 5-F

# NATIONAL TRANSPORTATION SAFETY BOARD

## Washington D.C.

### Weather Radar Data

# Index

U.S. DEPARTMENT OF COMMERCE / National Oceanic and Atmospheric Administration

OFCM

OFFICE OF THE FEDERAL COORDINATOR FOR
METEOROLOGICAL SERVICES AND SUPPORTING RESEARCH

FEDERAL METEOROLOGICAL HANDBOOK NO. 11

# DOPPLER RADAR METEOROLOGICAL OBSERVATIONS

## PART D
## WSR-88D UNIT DESCRIPTION AND OPERATIONAL APPLICATIONS

FCM-H11D-1992
(Interim Version One)


Washington, D.C.
April 1992

velocities. This is usually a second order effect.

Spectrum width values widen significantly and Doppler velocities become erratic in areas with very low signal-to-noise ratios.

**4.18 Microbursts.** Microbursts occur when a negatively buoyant column of air descends rapidly to the ground and spreads out on the surface omnidirectionally. Microbursts may occur in the absence of precipitation when ice crystals in virga evaporate into the environmental air, or in thunderstorms when updraft support is cut off from the hydrometeors suspended at midlevels.

**4.18.1 Recognition of Microbursts.** Microbursts are detectable by the WSR-88D either due to the density gradient or particulate matter, or both. In the reflectivity field, an annulus will be detected due to enhanced return from particulate matter and density gradients. Enhanced values may be as high as 10 $dBZ_e$. The spectrum width field may also show an anulus due to the turbulence along the outflow boundary. Spectrum width values of 8 to 12 knots are common.

A microburst will produce a unique signature detectable at low levels in the velocity field. A divergence couplet (i.e., a pattern of strong flow toward the radar, matched by an opposite pattern of strong flow away from the radar) will be seen on the display (Figure 2-13, Part C, this Handbook). At times this couplet can be distorted by the motion of the storm superimposed on the microbursts. In this situation, either the velocity toward or away from the radar will be higher than its opposite. The strong outflow from a microburst descends very close to the ground before spreading out and this spreading out in the velocity field might also be detectable in a Mean Radial Velocity Cross Section product. When descending air is translating along the radial, the resulting return will appear as either toward the radar or away from the radar. Divergence maximizes after about 3 to 5 minutes with a diameter of approximately 2.5 nmi and a velocity difference of up to 100 knots.

Through its radial component, the Combined Shear product will also display a signature if the specified resolution is 0.54 nmi or less (Figure 2-3, Part C, this Handbook).

**4.18.2 Considerations.** Due to the shallow vertical extent of the outflow from a microburst, this phenomenon will usually not be detected beyond the range of about 20 nmi. In addition, because of the short-lived nature of the microburst phenomenon (typically 3 to 5 minutes) and the scanning strategies used in the WSR-88D, microbursts may be infrequently detected at their maximum divergent signature.

At ranges nearer the radar, the Mean Radial Velocity product may prove most useful. At further distances from the radar, microbursts may be anticipated by monitoring high reflectivity cores at midlevels (16,000 to 40,000 feet) and watching for their descent. Collapsing echo tops or rapidly diminishing Vertically Integrated Liquid Water values



2

may also indicate such an event. However, the collapse of some storms results in only weak outflow.

A advantage of the Combined Shear product is that it detects the microburst signature independent of the translation of velocity.

**4.19 Considerations for Building a Routine Product Set.** The following information is intended as guidance to users with non-collocated PUPs in setting up Routine Product Set lists and is subject to modification by agency unique operational requirements.

The PUP provides the user the capability to define ten unique RPS lists, labeled A through J. Product sets A and B are invoked automatically whenever the radar changes operating modes, Precipitation and Clear Air, respectively. The user may replace either RPS A or B with a set stored in C through J. No set may contain more than 20 products.

**4.19.1 Clear Air Mode.** Due to the slow scan rate, most of the products on the RPS list can be base products. The user may include a 16-level, low-elevation clear air base Reflectivity product and an 8-level, long range Reflectivity product. Such derived products as the Velocity Azimuth Display Wind Profile and Echo Tops Products may also be added. Generally, there is time to handle one-time requests for other products.

**4.19.2 Precipitation Mode.** Building RPS lists for VCPs 11 and 21 can be complex. Conditions that influence the selection of products are the type, severity, range, and areal extent of the precipitation. In addition, the support being provided to other WSR-88D sites may be a factor in building the RPS.

With severe storms occurring at long range, especially if support is being provided to another site, the RPS list should concentrate on low-elevation base products at the highest resolution. The Storm Tracking Information product, which provides coverage out to 186 nmi, may be added. If storms are between 62 nmi and 124 nmi, velocity-derived products such as Mesocyclone and Storm Relative Mean Radial Velocity Map may be included. Since the data compaction techniques are more efficient when the area of coverage is small, the RPS list can consist mainly of base products without inducing load shedding. One-time requests for such products as Weak Echo Region, Cross Sections, and Storm Relative Mean Radial Velocity Region may also be accomplished without inducing load shedding. (The use of VCP 21 will allow the user more time to make one-time requests as well as providing good resolution of base products.) The lowest five elevation scans for both VCPs 11 and 21 are identical in supporting the hydrology algorithms and will cover storms at long range.

An RPS list for convective precipitation at short to medium ranges should be built around VCP 11. This will optimize algorithm performance and provide intermediate elevation scans for detailed analyses of storms using the Severe Weather Analysis, Cross Section, Weak Echo Region and Combined Moment products. The RPS list should include one



3

U.S. DEPARTMENT OF COMMERCE / National Oceanic and Atmospheric Administration

OFCM

OFFICE OF THE FEDERAL COORDINATOR FOR
METEOROLOGICAL SERVICES AND SUPPORTING RESEARCH

FEDERAL METEOROLOGICAL HANDBOOK NO. 11

# DOPPLER RADAR METEOROLOGICAL OBSERVATIONS

## PART B

## DOPPLER RADAR THEORY AND METEOROLOGY

FCM-H11B-1990
(Interim Version One)


Washington, D.C.
June 1990

4

additional range-dependent, site-varying correction is also applied to the precipitation rate data (Ahnert et al., 1983).

When the radome that encloses the radar antenna is wet, attenuation of the radar signal increases. This increased attenuation is a function of water film thickness and radar wavelength and may approach 1 dB for the WSR-88D. Because this temporary condition is difficult to describe quantitatively and because recovery is rapid once precipitation has ended, usually no attempt is made to account for this loss for S-band radars. Since wet radome attenuation introduces systematic bias, adjustment with rain gage data should help.

**5.3.2 Variations in the Z-R Relationship.** Many studies of the relationship between Z and R have been made, especially for rain. If the particle size distribution were a unique function of the precipitation rate, a universal Z-R relationship for rain would exist. However, it has been amply demonstrated that there is no unique particle size distribution for a given precipitation rate. The literature on the subject of Z-R relationships for rain is too extensive to be reviewed in detail in this section, however some of the more significant results are discussed below.

One of the original and most familiar relations is:

$$Z = 200R^{1.6} \tag{5-7}$$

following work of Marshall and Palmer (1948).

Numerous measurements of drop size distributions have been made in stratiform rain, rain showers, and thundershowers; and the characteristic Z-R relationships are reported in the literature [Battan (1973), Table 7.1, for a partial listing]. Ordinarily the coefficient in Eq. (5-6) increases as the precipitation becomes more convective. For example, Joss et al. (1970) gave:

$$\text{Drizzle} \qquad Z = 140R^{1.5} \tag{5-8}$$

$$\text{Thundershowers} \qquad Z = 500R^{1.5} \tag{5-9}$$

The presence of more large raindrops in thunderstorms causes the coefficient to be larger.

Drop size measurements beneath a large Oklahoma thunderstorm (Martner, 1977) yielded these relationships:

$$\text{Leading portion} \qquad Z = 667R^{1.33} \tag{5-10}$$

$$\text{Central core} \qquad Z = 124R^{1.64} \tag{5-11}$$

$$\text{Trailing portion} \qquad Z = 436R^{1.43} \tag{5-12}$$

A mean Z-R relationship for snow, where R is an equivalent rain rate, is:

$$Z = 2000R^{2} \tag{5-13}$$



Part B

Hail Z-R relationships depend upon the stone density, i.e., whether growth has been dry or wet, and the thickness of water films. Douglas (1963) found:

$$\text{Wet growth} \qquad Z = 84000R^{1.29} \tag{5-14}$$

$$\text{Dry growth} \qquad Z = 22500R^{1.17} \tag{5-15}$$

Considering all of the above, the coefficient and exponent in the Z-R relationship used with the WSR-88D hydrologic software are adaptable parameters with default values set at:

$$Z = 300R^{1.4} \tag{5-16}$$

Figure 5-1 gives examples of Z-R relationships for various forms of precipitation. As can be seen in Figure 5-1, use of Eq. (5-16) with the WSR-88D hydrologic software should provide a good average for different precipitation types.

The coefficient chosen in Eq. (5-16) is not as critical as one may expect, since a mean bias adjustment by the hydrologic software, using gage data, will be made. Of course this assumes that a reasonable number of rain gages are available under the radar umbrella to satisfactorily remove the mean bias. Also, assuming that the mean bias is removed, the error associated with the exponent is not excessive if a nominal value is chosen (e.g., 1.4) since errors caused by the Z-R relationship tend to cancel as data are averaged over greater space and time scales as shown in Figure 5-2 (Hudlow and Arkell, 1978).

Physical mechanisms that can alter particle size distribution and, consequently, a Z-R relationship include: evaporation, accretion, coalescence, breakup, size sorting, and vertical wind motion. Non-spherical ice particles and the flattening of raindrops as their size increases can enhance or reduce radar reflectivity measurements several decibels, depending on the radar polarization, and contribute errors to estimates of the precipitation rate. Mixed precipitation types, e.g., rain and hail in thunderstorms, can significantly alter a Z-R relationship. One means of minimizing the hail effect is to impose a maximum threshold on the precipitation rate. The threshold should be based on a maximum precipitation rate that can be expected in a given area. The presence of radar echoes beyond the threshold would then indicate the probability of hail and that specified upper limits of precipitation rate should not be exceeded.

Attempts have been made to determine Z-R variations based on other meteorological information such as storm type and weather conditions; however, limited benefit was derived for reducing precipitation rate uncertainty (Stout and Mueller, 1968).

**5.3.3 Time and Space Averaging.** WSR-88D data are obtained by scanning in azimuth at a series of low elevation angles and making measurements at discrete range and angular intervals. The equivalent reflectivity factor values are converted to rainfall rate with an appropriate Z-R relationship and accumulated in time to yield a spatial distribution of precipitation depth.

Regardless of the Z-R relationship used, this procedure results in time and space sampling errors. Figure 5-3 illustrates the increase in these errors as the sampling interval is increased over the various averaging areas. For example, the top graph in Figure 5-3 shows for this data set that

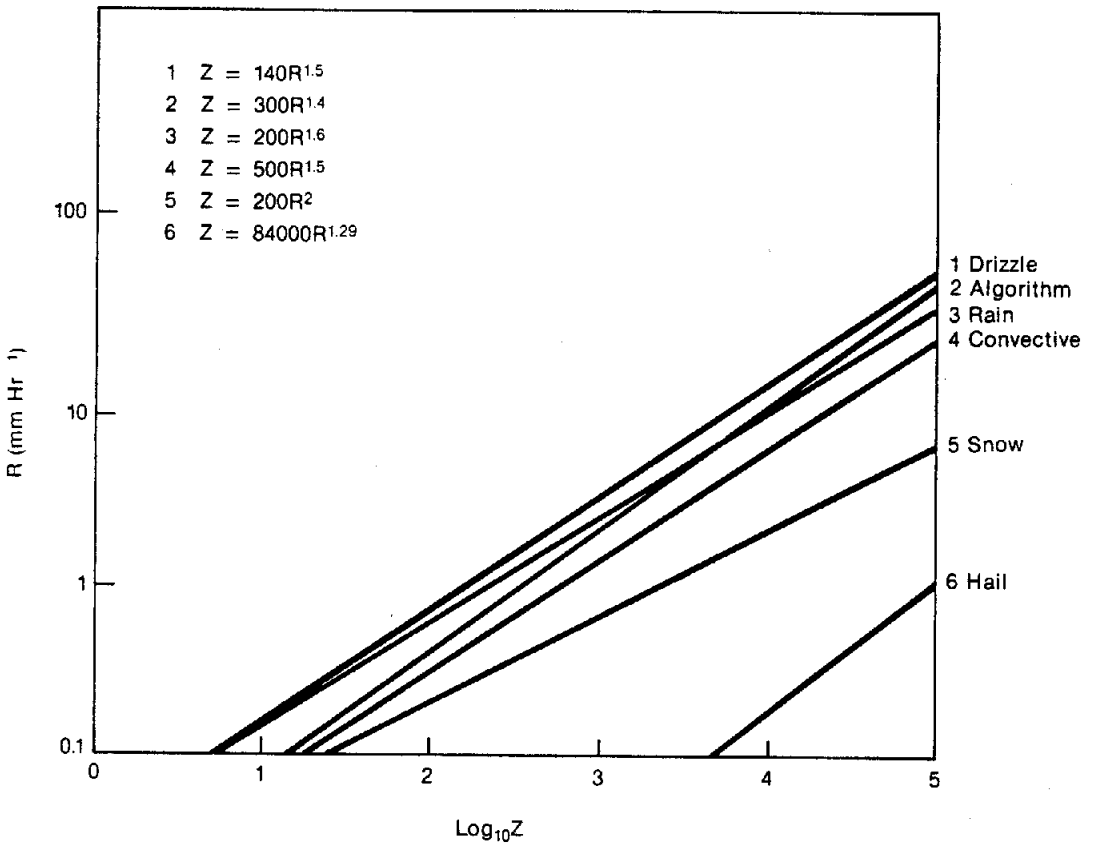


**Figure 5-1**
**Plots of Z-R Relationships Illustrate The Variability of Various Forms of Precipitation**



Part B

(7)

U.S. DEPARTMENT OF COMMERCE / National Oceanic and Atmospheric Administration

OFCM

OFFICE OF THE FEDERAL COORDINATOR FOR
METEOROLOGICAL SERVICES AND SUPPORTING RESEARCH

FEDERAL METEOROLOGICAL HANDBOOK NO. 11

# DOPPLER RADAR METEOROLOGICAL OBSERVATIONS

PART C
WSR-88D PRODUCTS
AND ALGORITHMS


FCM-H11C-1991
(INTERIM VERSION ONE)

Washington, D.C.
February 1991

**3.9 Vertically Integrated Liquid Water.** The Vertically Integrated Liquid (VIL) Water algorithm converts weather radar reflectivity factor data into liquid-water content values based on theoretical studies of drop-size distributions and empirical studies of the relationship between reflectivity factor and liquid-water content. The algorithm described uses an equation that relates reflectivity factor to liquid water content for one such relationship.

For each elevation angle, each 4 x 4 km (2.2 x 2.2 nmi) grid box is assigned the largest liquid-water value of all the sample volumes located within the grid box. All other liquid-water values in each grid box are ignored. This compensates for the fact that the storm may be tilted and moving during the time required for a complete volume scan. These partial liquid-water content values are then integrated vertically to arrive at VIL values for each grid box. If the VIL value for a grid box exceeds 80 x $10^6$ kg $km^{-2}$ it is adjusted to 80 x $10^6$ kg $km^{-2}$ to mitigate the large reflectivity values associated with hail.

**3.9.1 Operational Parameters.**

- Minimum Reflectivity Threshold--minus 33.0 to 94.0 $dBz_e$; default, 18.3 $dBZ_e$: Minimum reflectivity used in computing VIL.

- Maximum Liquid Water Threshold--1 to 200 kg $m^{-2}$; default, 80 kg $m^{-2}$: Threshold against which liquid water (integrated) is tested. Maximum allowable computed VIL value.

**3.9.2 Operational Considerations.** VIL's primary utility is in identifying strong storms that may become severe, especially those with hail. The magnitude of the estimated VIL is related to the strength of the updraft in a storm, and consequently to the storm's severe weather potential. Due to the parameters of the liquid-water content conversion equation, reflectivity factor values less than 40 $dBZ_e$ contribute little to a storm's VIL value. storms.

Varying drop-size distributions, the presence of hail, overshooting low-level precipitation, beam broadening with range, and non-vertically contiguous volume coverage patterns may all affect the accuracy of the VIL calculation for any given storm, although the effect may be beneficial in the case of hail. The effects due to the volume coverage pattern will depend on several factors: height of the storm, distance of the storm from the radar, and the vertical distributions of reflectivity within the storm. Figure 3-3 exhibits the resultant VIL values for a single stationary, vertical storm at various ranges using different volume coverage patterns. Another potential weakness is that the VIL grid box dimensions of 4 x 4 km (2.2 x 2.2 nmi) are too small for those cases where a storm is strongly tilted with height or is moving very rapidly. For those storms, the calculated VIL will be lower than the true "storm" VIL.

An important consideration is the need to quantify the regional, seasonal, diurnal, and airmass variations in VIL magnitude versus severe weather. Under differing meteorological conditions, the minimum VIL associated with severe weather may vary considerably. Warm, moist environments tend to require higher VIL values for severe weather occurrences than cool, dry conditions. Operational usage in Oklahoma has indicated that critical VIL values there can vary from 35 x $10^6$ kg $km^{-2}$ in late fall or winter to 60 x $10^6$ kg $km^{-2}$ in summer. These guidelines, along with operational experience, may help to identify appropriate VIL thresholds for each WSR-88D site.

Part C

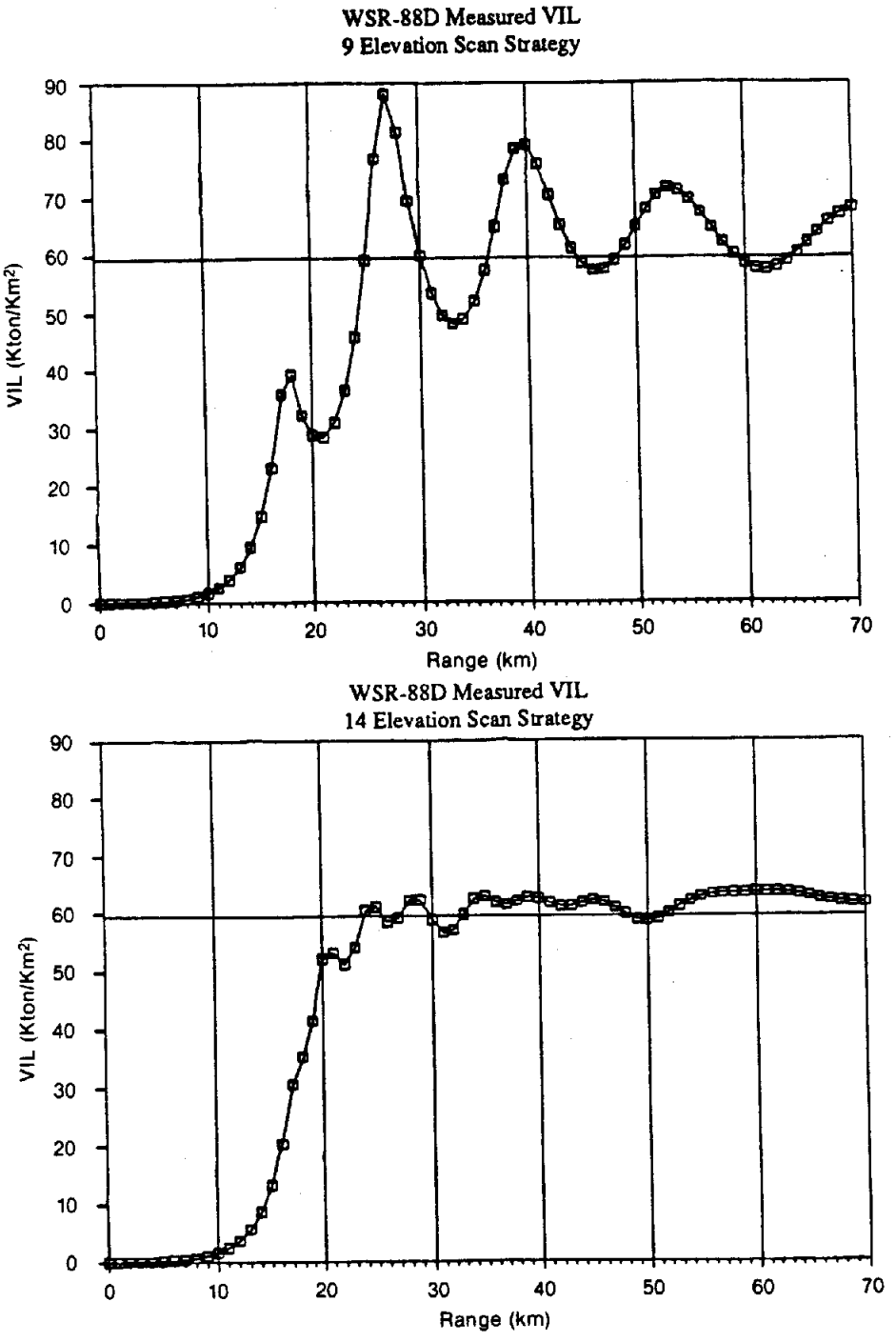


**Figure 3-3**
**VIL Values for a Single Storm as a Function of Range**

**(Mahoney, 1987)**

Part C

UDC 551.501.81:551.509.54:551.576

# Vertically Integrated Liquid Water—A New Analysis Tool

**DOUGLAS R. GREENE**—*Techniques Development Laboratory, NOAA, Silver Spring, Md.*

**ROBERT A. CLARK**—*Department of Meteorology, Texas A&M University, College Station, Tex.*

**ABSTRACT**—Through the use of digital radar data measured at successive elevation angles in a storm system, we developed a technique that presents a new dimension in mesoscale analysis. This technique, mapped vertically integrated liquid-water content (VIL), presents the three-dimensional characteristics of a storm system in a two-dimensional display. This analysis technique appears to hold real promise for both severe storm and hydrologic applications.

## 1. INTRODUCTION

The space-time density of regular synoptic meteorological data is inadequate for many meteorological purposes. This data gap is partially filled by weather radars that can effectively scan a radius of 100 mi and, in some cases, an entire storm-producing area. In most cases, these radar data are reduced manually by field forecasters for short-range forecasting and issuing of storm warnings (Bigler et al. 1970). Manual techniques are frequently impractical because (1) the large quantities of data generated by the radar are too difficult to assimilate and (2) the visual extrapolation of radar data is often unreliable because of rapid changes in small-scale echo characteristics. The ultimate solution is "real-time" automatic computer processing and analysis of radar data. Steps were taken toward a real-time system with the development of the digitizing hardware and procedures for the WSR–57 by the National Severe Storms Laboratory (NSSL) of the National Oceanic and Atmospheric Administration (NOAA) and by the initiation in spring 1971 of an experiment in digitizing weather radar data from a four-station network by the National Weather Service (NWS), NOAA. Digital radar data have been used for hydrologic applications and by Barclay and Wilk (1970) to identify and track storms. However, the full potential of these data has not been fully exploited.

We are currently studying the feasibility of utilizing digital radar data for severe weather forecasting and hydrologic applications. The purpose of this paper is to preview some of our experiments and to report an analysis technique that presents a new dimension in the analysis of radar data.

## 2. DATA

Digital radar data used in this study were furnished by NSSL. The techniques used in the collection, processing, and recording of these data have been described in detail by Wilk et al. (1967). These data are presented in digital form for each 2° of azimuth at 1 n.mi. ranges for successive elevation angles in steps of one beam width (2°). By using the calibration data supplied in the digital record one can convert these data to normalized power or radar reflectivity. It is frequently desirable to convert these data from the radar coordinate system to a system having the vertical direction as a coordinate. As part of our work we have studied various coordinate systems, interpolation procedures, and grid intervals that will be reported on in a future paper. The analyses presented in this paper were performed by use of a quadratic interpolation procedure in a cylindrical coordinate system having a 2°×1 n.mi. ×5,000-ft grid interval. This coordinate system minimizes errors since interpolation is required only for the vertical coordinate.

## 3. CAZM PRESENTATIONS

If digital radar data are available for successive elevation angles in steps of one beam width, it is possible to construct constant altitude reflectivity maps (CAZM) for any desired level within the range of the data (figs. 1–3). On these maps, radar reflectivity, $Z$, values are expressed in dbZs; that is, the value plotted is 10 log $Z$, where $Z$ is expressed in $m^6 \cdot m^{-3}$. These maps are similar to the constant altitude plan position indicator (CAPPI) presentations developed by Marshall at McGill University (Wein 1963). CAZM presentations in figures 1–3 clearly illustrate the storm intensity at three selected levels, thus allowing a three-dimensional interpretation of the echoes.[1] These presentations are very useful in mesoanalysis and/or the study of thunderstorm dynamics. Although a CAZM illustrates the echo or storm intensity at various constant levels, to identify precisely the most intense echoes, one must look at the CAZM for each level and integrate mentally the intensities through the depth of the storm. An analysis technique and display that presents this three-dimensional characteristic in a two-dimensional display is presented in the next section.

[1] Technically, figure 1 is not a CAZM but is a map of 0° reflectivity.

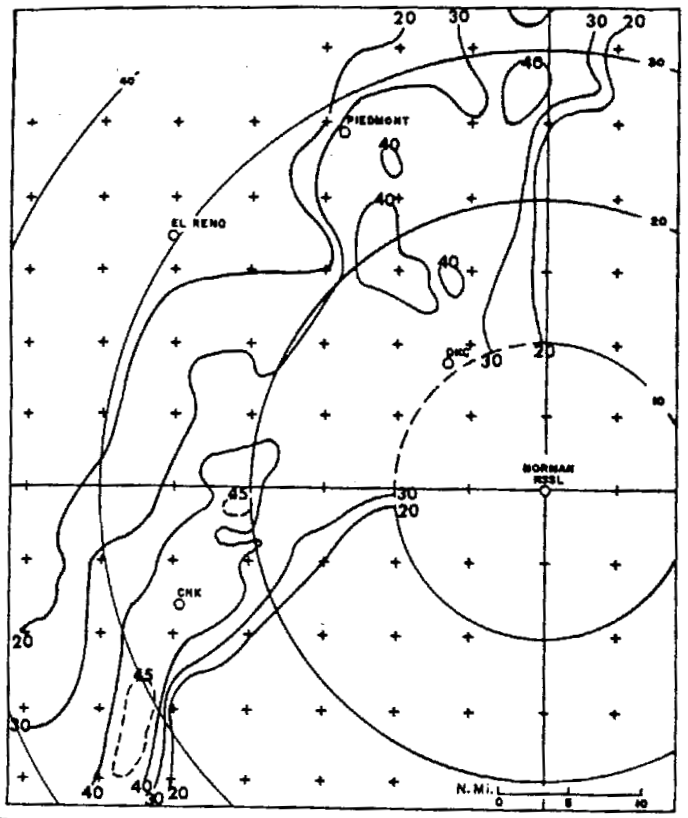


FIGURE 1.—Zero-degree reflectivity in dbZs for 1650 CST, Apr. 26, 1969.

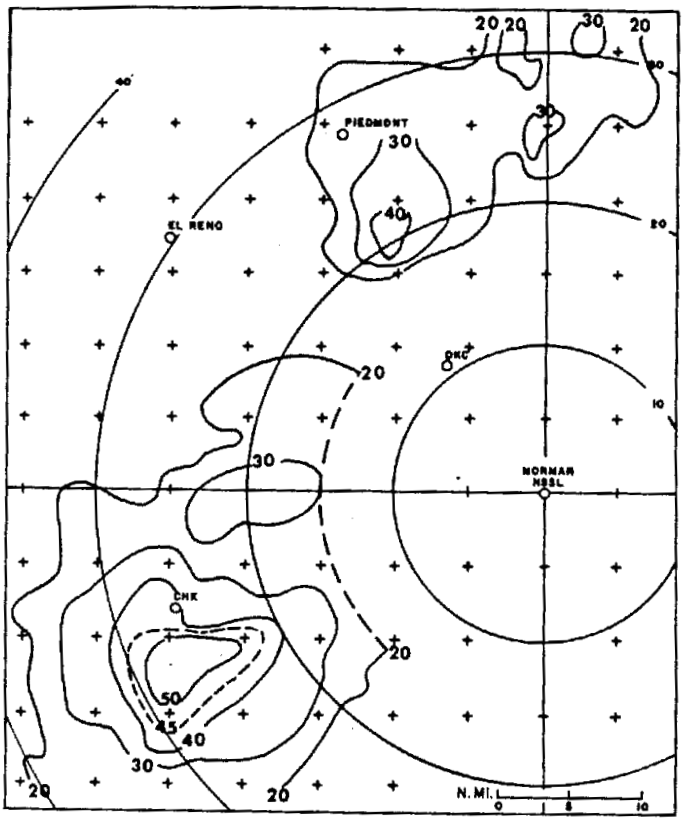


FIGURE 3.—CAZM at 30,000 ft for 1650–57 CST, Apr. 26, 1969

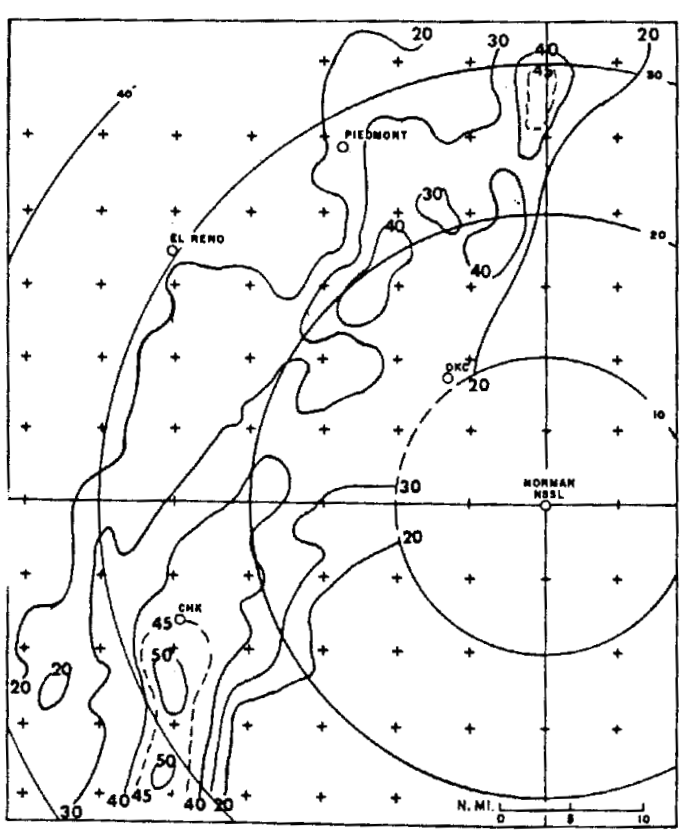


FIGURE 2.—CAZM at 10,000 ft for 1650–57 CST, Apr. 26, 1969.

## 4. VERTICALLY INTEGRATED LIQUID-WATER CONTENT (VIL)

The concentration of liquid water in a cloud is of considerable meteorological importance. Its magnitude and spatial distribution are important factors in the study of cloud dynamics since they indicate the degree of condensation and development that has taken place. Changes in the water content are important thermodynamically because they are accompanied by large energy changes (Mason 1957). Unfortunately, at this time there is no method of rapidly and accurately measuring the magnitude of liquid-water content; however, its relative magnitude and distribution may be determined by radar measurements if certain assumptions are made regarding the in-cloud drop-size distribution. An exponential drop-size distribution proposed by Marshall and Palmer (1948) seems to fit the distributions observed by several investigators. This distribution is given by

$$n(a)=N_0 \exp(-ba) \qquad (1)$$

where $a$ is the drop diameter, $n(a)$ is the number of drops of diameter $a$, and $N_0$ and $b$ are parameters in the distribution.

To use radar as an indicator of liquid-water content, $M$, a relationship was obtained between $M$ and radar reflectivity, $Z$. Mathematically, $M$ and $Z$ may be defined by

$$M=\frac{\rho_w \pi}{6}\int_0^\infty n(a)a^3 da$$



469-748 O - 72 - 5

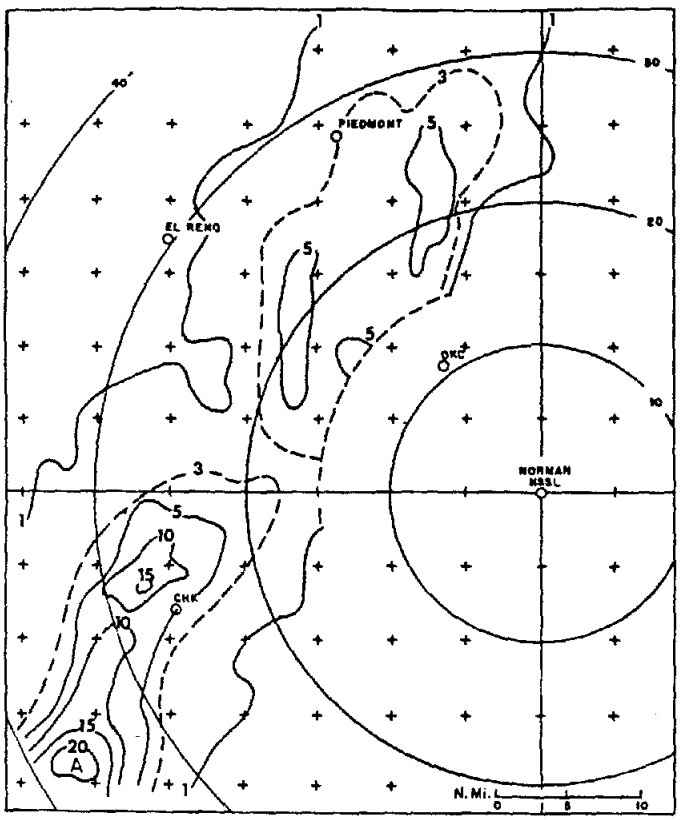


FIGURE 4.—VIL map for 1640–47 CST, Apr. 26, 1969. Isopleths of $M^*$ are in kg·m$^{-2}$.

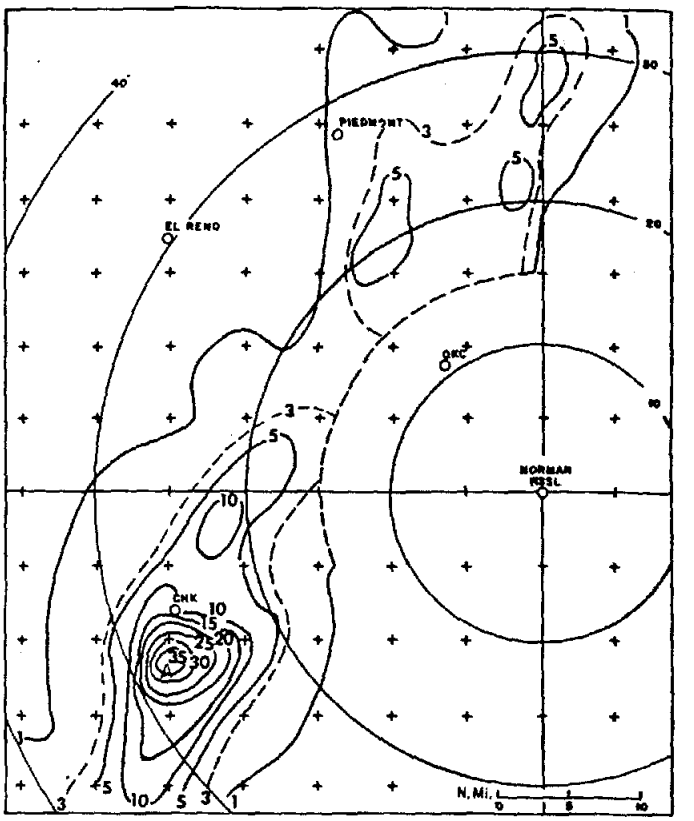


FIGURE 5.—VIL map for 1650–57 CST, Apr. 26, 1969. Isopleths of $M^*$ are in kg · m$^{-2}$.

and

$$Z=\int_0^x n(a)a^6da \tag{3}$$

where $x$ is the maximum drop diameter and $\rho_w$ is the density of water. When the Marshall-Palmer drop-size distribution is used in eq (2) and (3), the error is small if the upper limit of integration, $x$, is replaced by $\infty$. Integration yields

$$M=\frac{N_0\rho_w\pi}{6}\int_0^\infty \exp(-ba)\ a^3da=\frac{N_0\rho_w\pi}{6}\frac{\Gamma(4)}{b^4}=\frac{N_0\rho_w\pi}{b^4} \tag{4}$$

and

$$Z=N_0\int_0^\infty \exp(-ba)\ a^6\,da=\frac{N_0\Gamma(4)}{b^7}=\frac{720N_0}{b^7}. \tag{5}$$

Eliminating the parameter $b$ between eq (4) and (5) yields

$$M=\frac{N_0\pi\rho_w}{[720\times 10^{18}N_0]^{4/7}}Z^{4/7}. \tag{6}$$

For $N_0=8\times 10^6\text{m}^{-4}$ and $\rho_w=10^6$ g/m$^3$,

$$M=3.44\times 10^{-3}\,Z^{4/7} \tag{7}$$

where the units of $M$ are g·m$^{-3}$ and of $Z$ are mm$^6$·m$^{-3}$. The factor of $10^{18}$ in the denominator in eq (6) is required to convert the units of $Z$ from m$^6$·m$^{-3}$ as given in eq (5) to mm$^6$·m$^{-3}$.

$M^*$ is defined as the vertically integrated liquid-water content of the storm and has units of mass per unit area. $M^*$ is computed by integrating eq (7) from the base to the top of the echo; that is,

$$M^*=\int_{h_{base}}^{h_{top}}Mdh'=3.44\times 10^{-6}\int_{h_{base}}^{h_{top}}Z^{4/7}dh' \tag{8}$$

where $h'$ is the height expressed in meters and $M^*$ has units of kg·m$^{-2}$. It should be noted that $M$ and $M^*$ represent the mass of raindrops in a unit volume and unit area, respectively. Since $M^*$ is based on the relationship between $M$ and $Z$, it would be incorrect to assume that $M^*$ denotes all the in-cloud liquid water. Clouds containing a large number of small drops produce very small values of $Z$, which may be below the detectable signal of the WSR–57 radar, thus some liquid-water content, $M$, will not be detected. Hail may also produce fictitious values of liquid water due to enhanced radar return. However, this may be beneficial as an indicator of the severity of a storm.

VIL charts computed from digital radar data collected by NSSL during a storm event on Apr. 26, 1969, are presented in figures 4 and 5. The 5-min isohyetal maps corresponding to these times are presented in figures 6 and 7. The time of the isohyetal map in figure 7 corresponds to the 0° elevation $Z$ map (fig. 1) and the VIL on figure 5. Since the VIL maps integrate over all levels, the configuration of echoes in figures 1–3 and that in figure 5 will be somewhat different. Values of $M^*$ below 1 kg·m$^{-2}$ were not depicted in figures 4 and 5. Visual comparison of these figures indicates that the VIL is possibly a better indicator of rainfall than 0° radar reflectivity. Detailed studies are currently being made to investigate the correlation of rainfall rate, $R$, with $M^*$.

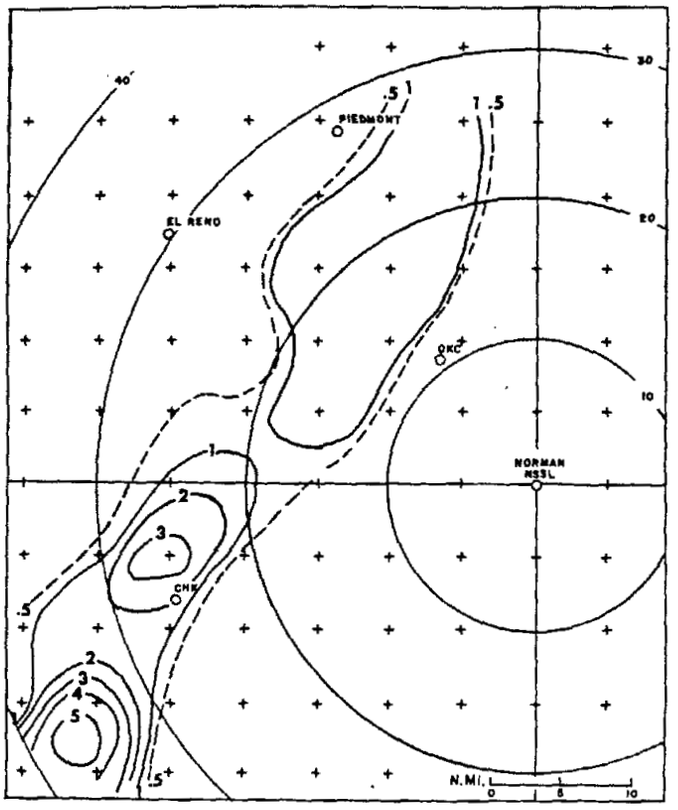


FIGURE 6.—Five-min rainfall rate, $R$ (in./hr), for 1640–45 CST, Apr. 26, 1969.

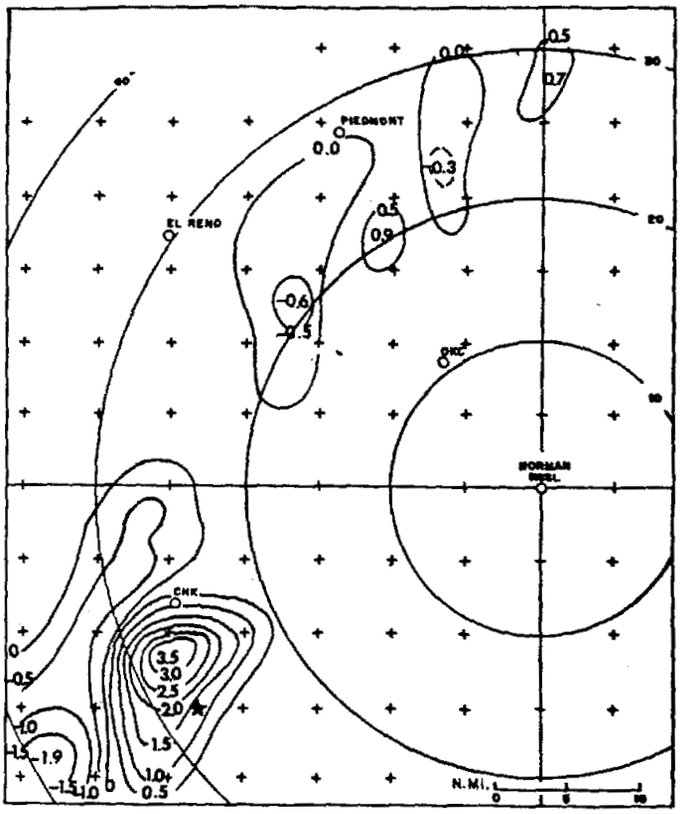


FIGURE 8.—Total change in $M^*$ between 1640 and 1650 CST, Apr. 26, 1969. Isopleths are in kg · m$^{-2}$ · min$^{-1}$. The star indicates the approximate location of a confirmed tornado.

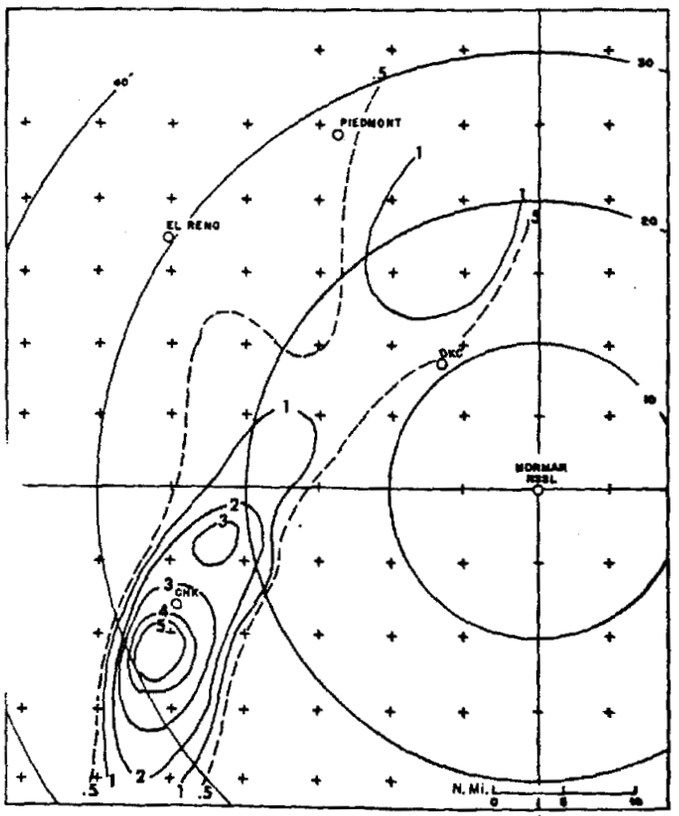


FIGURE 7.—Five-min rainfall rate, $R$ (in./hr), for 1650–55 CST, Apr. 26, 1969.

VIL analyses also provide a new means for identification and possible forecasting of severe storms. The local change in $M^*$ (i.e., $\partial M^*/\partial t$) for the time interval between the maps in figures 4 and 5 is shown in figure 8. It is of interest to note that, in a 10-min interval, the maximum $M^*$ in echo A (figs. 4, 5)i ncreased from 20 kg·m$^{-2}$ to 35 kg·m$^{-2}$. This rapid increase in liquid-water content appears to be an indicator of "explosive development" of severe storms. At 1700 CST, just after this marked increase in $M^*$, a confirmed tornado occurred at the location of the star in figure 8. This suggests that the trend in $M^*$ may be an indicator of severe weather development. Other cases with tornado occurrences are being studied to test this hypothesis.

There are many possible applications of the VIL analyses. For example, $M^*$ may be computed from tilt digital data obtained from the national network of radar stations and a composite VIL formed. This composite would have many advantages over the present National Radar Summary Chart (NWS) because it would present an integrated three-dimensional display depicting the character and intensity of all storms in the network. The temporal nature of storm systems can be indicated by successive VIL's or by maps of $\partial M^*/\partial t$ similar to figure 8. This would approach the ultimate goal of the National Radar Network Display.

Although a large-scale digital computer was used to produce the VIL maps presented in this paper, with proper ordering of data, $M^*$ values could be computed

on a "mini" computer at the radar site. Thus, $M^*$ values would be readily available for real-time use.

Another advantage of vertically integrated values is that vertical integration will filter out strong radar returns that may be due to terrain features or nonstandard propagation. Although these returns may be very strong at low elevation angles, thus adversely affecting present $Z$–$R$ relationships, they become insignificant when integrated over the vertical extent of the storm.

## 5. CONCLUSIONS

This preliminary investigation indicates that radar tilt data collected over short time intervals may prove to be very beneficial in both hydrologic and severe storm analyses. It is apparent that data collected at constant low antenna elevation angles may not reveal the complete character of a storm. A measure, such as total liquid water, yields an integrated morphology of severe storm systems.


### ACKNOWLEDGMENTS

The authors are grateful to NSSL staff members—in particular Edwin Kessler, Ken E. Wilk, and Kathryn Gray for their helpful comments on digital data processing and for providing us with the data used in this study. Acknowledgment is extended to the U.S. Army Electronic Command for Contract DAAB07-68-C-0073 (Project Themis) which provided the funds for computer rental and data reduction. Portions of this work by the senior author are in partial fulfillment of requirements for the doctoral degree in meteorology at Texas A&M University.


### REFERENCES


Barclay, Peter A., and Wilk, Kenneth E., "Severe Thunderstorm Radar Echo Motion and Related Weather Events Hazardous to Aviation Operations," *ESSA Technical Memorandum* ERLTM-NSSL 46, U.S. Department of Commerce, National Severe Storms Laboratory, Norman, Okla., June **1970**, 62 pp.

Bigler, Stuart G., McGrew, Russell G., and St. Clair, J. Michael, "An Experiment in Digitizing Weather Radar Data From a Four Station Network," *Proceedings of the Fourteenth Radar Meteorology Conference, Tucson, Arizona, November 17–20, 1970*, American Meteorological Society, Boston, Mass., **1970**, pp, 395–398.

Marshall, John Stewart, and Palmer, Wayne McK., "The Distribution of Raindrops With Size," *Journal of Meteorology*, Vol. 5, No. 4, Aug. **1948**, pp. 165–166.

Mason, Basil John, *The Physics of Clouds*, Oxford University Press, London, England, **1957**, 481 pp.

Wein, Marceli, "Facsimile Output for Weather Radar," *Proceedings of the Tenth Weather Radar Conference, Washington, D.C., April 22–25, 1963*, American Meteorological Society, Boston, Mass., Apr. **1963**, pp. 365–369.

Wilk, Kenneth E., Watts, Walter L., Sirmans, Dale, Lhermitte, Roger M., Kessler, Edwin, and Gray, Kathryn C., "Weather Radar Data System at the National Severe Storms Laboratory," Preprint of paper presented at the Fifth Conference on Severe Local Storms, St. Louis, Missouri, October 19–20, **1967**, pp. 14–23 (unpublished manuscript).



*[Received July 12, 1971; revised February 1, 1972]*




15

HEIGHT OF CENTER OF RADAR BEAM; ROUNDED TO NEAREST 1000 FEET (KFT); TRUNCATED AT 70 KFT

CALCULATED FROM $H = (SR*SIN(EL) + SR^2*COS^2(EL)/CONSTANT)*6.076$
WHERE: SR = SLANT RANGE; EL =ELEVATION ANGLE; CONSTANT = 9169 (BASED ON 4/3 EARTH MODEL)

| | SLANT RANGE (N MI) | | | | | | | | | | | | | | | | | | | | | | |
|---|---|---|---|---|---|---|---|---|---|---|---|---|---|---|---|---|---|---|---|---|---|---|---|
| ELEVATION | 5 | 10 | 15 | 20 | 25 | 30 | 40 | 50 | 60 | 70 | 80 | 90 | 100 | 110 | 120 | 130 | 140 | 150 | 160 | 170 | 180 | 190 | 200 |
| 0 | 0 | 0 | 0 | 0 | 0 | 1 | 1 | 2 | 2 | 3 | 4 | 5 | 7 | 8 | 10 | 11 | 13 | 15 | 17 | 19 | 21 | 24 | 27 |
| 0.5 | 0 | 1 | 1 | 1 | 2 | 2 | 3 | 4 | 6 | 7 | 8 | 10 | 12 | 14 | 16 | 18 | 20 | 23 | 25 | 28 | 31 | 34 | 37 |
| 1 | 1 | 1 | 2 | 2 | 3 | 4 | 5 | 7 | 9 | 11 | 13 | 15 | 17 | 20 | 22 | 25 | 28 | 31 | 34 | 37 | 41 | 44 | 48 |
| 1.5 | 1 | 2 | 3 | 3 | 4 | 5 | 7 | 10 | 12 | 14 | 17 | 20 | 23 | 26 | 29 | 32 | 35 | 39 | 42 | 46 | 50 | 54 | 58 |
| 2 | 1 | 2 | 3 | 5 | 6 | 7 | 10 | 12 | 15 | 18 | 21 | 24 | 28 | 31 | 35 | 39 | 43 | 47 | 51 | 55 | 60 | 64 | 69 |
| 3 | 2 | 3 | 5 | 7 | 8 | 10 | 14 | 18 | 21 | 25 | 30 | 34 | 38 | 43 | 48 | 53 | 57 | 63 | 68 | 70 | 70 | 70 | 70 |
| 4 | 2 | 4 | 7 | 9 | 11 | 13 | 18 | 23 | 28 | 33 | 38 | 43 | 49 | 55 | 60 | 66 | 70 | 70 | 70 | 70 | 70 | 70 | 70 |
| 5 | 3 | 5 | 8 | 11 | 14 | 16 | 22 | 28 | 34 | 40 | 47 | 53 | 60 | 66 | 70 | 70 | 70 | 70 | 70 | 70 | 70 | 70 | 70 |
| 6 | 3 | 6 | 10 | 13 | 16 | 20 | 26 | 33 | 40 | 48 | 55 | 62 | 70 | 70 | 70 | 70 | 70 | 70 | 70 | 70 | 70 | 70 | 70 |
| 7 | 4 | 7 | 11 | 15 | 19 | 23 | 31 | 39 | 47 | 55 | 63 | 70 | 70 | 70 | 70 | 70 | 70 | 70 | 70 | 70 | 70 | 70 | 70 |
| 8 | 4 | 9 | 13 | 17 | 22 | 26 | 35 | 44 | 53 | 62 | 70 | 70 | 70 | 70 | 70 | 70 | 70 | 70 | 70 | 70 | 70 | 70 | 70 |
| 9 | 5 | 10 | 14 | 19 | 24 | 29 | 39 | 49 | 59 | 70 | 70 | 70 | 70 | 70 | 70 | 70 | 70 | 70 | 70 | 70 | 70 | 70 | 70 |
| 10 | 5 | 11 | 16 | 21 | 27 | 32 | 43 | 54 | 66 | 70 | 70 | 70 | 70 | 70 | 70 | 70 | 70 | 70 | 70 | 70 | 70 | 70 | 70 |
| 11 | 6 | 12 | 18 | 23 | 29 | 35 | 47 | 60 | 70 | 70 | 70 | 70 | 70 | 70 | 70 | 70 | 70 | 70 | 70 | 70 | 70 | 70 | 70 |
| 12 | 6 | 13 | 19 | 26 | 32 | 38 | 52 | 65 | 70 | 70 | 70 | 70 | 70 | 70 | 70 | 70 | 70 | 70 | 70 | 70 | 70 | 70 | 70 |
| 13 | 7 | 14 | 21 | 28 | 35 | 42 | 56 | 70 | 70 | 70 | 70 | 70 | 70 | 70 | 70 | 70 | 70 | 70 | 70 | 70 | 70 | 70 | 70 |
| 14 | 7 | 15 | 22 | 30 | 37 | 45 | 60 | 70 | 70 | 70 | 70 | 70 | 70 | 70 | 70 | 70 | 70 | 70 | 70 | 70 | 70 | 70 | 70 |
| 15 | 8 | 16 | 24 | 32 | 40 | 48 | 64 | 70 | 70 | 70 | 70 | 70 | 70 | 70 | 70 | 70 | 70 | 70 | 70 | 70 | 70 | 70 | 70 |
| 16 | 8 | 17 | 25 | 34 | 42 | 51 | 68 | 70 | 70 | 70 | 70 | 70 | 70 | 70 | 70 | 70 | 70 | 70 | 70 | 70 | 70 | 70 | 70 |
| 17 | 9 | 18 | 27 | 36 | 45 | 54 | 70 | 70 | 70 | 70 | 70 | 70 | 70 | 70 | 70 | 70 | 70 | 70 | 70 | 70 | 70 | 70 | 70 |
| 18 | 9 | 19 | 28 | 38 | 47 | 57 | 70 | 70 | 70 | 70 | 70 | 70 | 70 | 70 | 70 | 70 | 70 | 70 | 70 | 70 | 70 | 70 | 70 |
| 19 | 10 | 20 | 30 | 40 | 50 | 60 | 70 | 70 | 70 | 70 | 70 | 70 | 70 | 70 | 70 | 70 | 70 | 70 | 70 | 70 | 70 | 70 | 70 |
| 20 | 10 | 21 | 31 | 42 | 52 | 63 | 70 | 70 | 70 | 70 | 70 | 70 | 70 | 70 | 70 | 70 | 70 | 70 | 70 | 70 | 70 | 70 | 70 |
| 21 | 11 | 22 | 33 | 44 | 55 | 66 | 70 | 70 | 70 | 70 | 70 | 70 | 70 | 70 | 70 | 70 | 70 | 70 | 70 | 70 | 70 | 70 | 70 |
| 22 | 11 | 23 | 34 | 46 | 57 | 69 | 70 | 70 | 70 | 70 | 70 | 70 | 70 | 70 | 70 | 70 | 70 | 70 | 70 | 70 | 70 | 70 | 70 |
| 23 | 12 | 24 | 36 | 48 | 60 | 70 | 70 | 70 | 70 | 70 | 70 | 70 | 70 | 70 | 70 | 70 | 70 | 70 | 70 | 70 | 70 | 70 | 70 |
| 24 | 12 | 25 | 37 | 50 | 62 | 70 | 70 | 70 | 70 | 70 | 70 | 70 | 70 | 70 | 70 | 70 | 70 | 70 | 70 | 70 | 70 | 70 | 70 |
| 25 | 13 | 26 | 39 | 52 | 65 | 70 | 70 | 70 | 70 | 70 | 70 | 70 | 70 | 70 | 70 | 70 | 70 | 70 | 70 | 70 | 70 | 70 | 70 |
| 26 | 13 | 27 | 40 | 53 | 67 | 70 | 70 | 70 | 70 | 70 | 70 | 70 | 70 | 70 | 70 | 70 | 70 | 70 | 70 | 70 | 70 | 70 | 70 |
| 27 | 14 | 28 | 41 | 55 | 69 | 70 | 70 | 70 | 70 | 70 | 70 | 70 | 70 | 70 | 70 | 70 | 70 | 70 | 70 | 70 | 70 | 70 | 70 |
| 28 | 14 | 29 | 43 | 57 | 70 | 70 | 70 | 70 | 70 | 70 | 70 | 70 | 70 | 70 | 70 | 70 | 70 | 70 | 70 | 70 | 70 | 70 | 70 |
| 29 | 15 | 30 | 44 | 59 | 70 | 70 | 70 | 70 | 70 | 70 | 70 | 70 | 70 | 70 | 70 | 70 | 70 | 70 | 70 | 70 | 70 | 70 | 70 |
| 30 | 15 | 30 | 46 | 61 | 70 | 70 | 70 | 70 | 70 | 70 | 70 | 70 | 70 | 70 | 70 | 70 | 70 | 70 | 70 | 70 | 70 | 70 | 70 |
| 34 | 17 | 34 | 51 | 68 | 70 | 70 | 70 | 70 | 70 | 70 | 70 | 70 | 70 | 70 | 70 | 70 | 70 | 70 | 70 | 70 | 70 | 70 | 70 |
| 38 | 19 | 37 | 56 | 70 | 70 | 70 | 70 | 70 | 70 | 70 | 70 | 70 | 70 | 70 | 70 | 70 | 70 | 70 | 70 | 70 | 70 | 70 | 70 |
| 42 | 20 | 41 | 61 | 70 | 70 | 70 | 70 | 70 | 70 | 70 | 70 | 70 | 70 | 70 | 70 | 70 | 70 | 70 | 70 | 70 | 70 | 70 | 70 |
| 46 | 22 | 44 | 66 | 70 | 70 | 70 | 70 | 70 | 70 | 70 | 70 | 70 | 70 | 70 | 70 | 70 | 70 | 70 | 70 | 70 | 70 | 70 | 70 |
| 50 | 23 | 47 | 70 | 70 | 70 | 70 | 70 | 70 | 70 | 70 | 70 | 70 | 70 | 70 | 70 | 70 | 70 | 70 | 70 | 70 | 70 | 70 | 70 |

Values of reflectivity, rainfall rate, and liquid water content for RADAP II and DVIP reflectivity intensity categories.

| RADAP CATEGORY | VIP CATEGORY | THRESHOLD Ze $mm^6/m^3$ | THRESHOLD LOG Ze | THRESHOLD dBZe | THRESHOLD DVIP 1/2 dBZe | THRESHOLD R(200)[1] in/hr | MIDPOINT Ze $mm^6/m^3$ | MIDPOINT LOG Ze | MIDPOINT R(200)[1] in/hr | MIDPOINT R(55)[2] in/hr | MIDPOINT M[3] $g/m^3$ |
|---|---|---|---|---|---|---|---|---|---|---|---|
| 1 | 1 | 68 | 1.83 | 18.5 | 37 | 0.02 | 182 | 2.26 | 0.04 | 0.08 | 0.0 |
| 2 | | 295 | 2.47 | 24.5 | 49 | 0.05 | 593 | 2.77 | 0.08 | 0.16 | 0.1 |
| 3 | 2 | 891 | 2.95 | 29.5 | 59 | 0.10 | 2140 | 3.33 | 0.17 | 0.39 | 0.3 |
| 4 | | 3388 | 3.53 | 35.5 | 71 | 0.23 | 5153 | 3.71 | 0.30 | 0.67 | 0.5 |
| 5 | | 6918 | 3.84 | 38.5 | 77 | 0.36 | 9309 | 3.97 | 0.44 | 0.97 | 0.6 |
| 6 | 3 | 11700 | 4.07 | 40.5 | 81 | 0.50 | 15150 | 4.18 | 0.59 | 1.32 | 0.8 |
| 7 | | 18600 | 4.27 | 42.5 | 85 | 0.67 | 19950 | 4.30 | 0.70 | 1.57 | 1.0 |
| 8 | | 21300 | 4.33 | 43.5 | 87 | 0.83 | 28400 | 4.45 | 0.87 | 1.94 | 1.2 |
| 9 | 4 | 35500 | 4.55 | 45.5 | 91 | 1.00 | 45850 | 4.66 | 1.18 | 2.63 | 1.6 |
| 10 | | 56200 | 4.75 | 47.5 | 95 | 1.33 | 67800 | 4.83 | 1.50 | 3.36 | 2.0 |
| 11 | | 79400 | 4.90 | 49.0 | 98 | 1.66 | 93200 | 4.97 | 1.84 | 4.11 | 2.4 |
| 12 | 5 | 107000 | 5.03 | 50.5 | 101 | 2.00 | 155500 | 5.19 | 2.52 | 5.64 | 3.2 |
| 13 | | 204000 | 5.31 | 53.0 | 106 | 3.00 | 264000 | 5.42 | 3.51 | 7.86 | 4.3 |
| 14 | | 324000 | 5.51 | 55.0 | 110 | 4.00 | 396000 | 5.60 | 4.55 | 7.86[4] | 5.4 |
| 15 | 6 | 468000 | 5.67 | 56.5 | 113 | 5.00 | | | 4.55[4] | 7.86[4] | 5.4[4] |

[1] $Z=200R^{1.6}$ [2] $Z=55R^{1.6}$ [3] $M=3.44\times10^{-3}Z^{4/7}$ [4] Lower values used to minimize hail effects

$Z=300R^{1.4}$